Earth and Planetary Science Letters 523 (2019) 115708

Contents lists available at ScienceDirect

Earth and Planetary Science Letters

www.elsevier.com/locate/epsl

Active crustal deformation in southeastern Tibetan Plateau: The kinematics and dynamics

Yujiang Li [a,b], Mian Liu [b,*], Yuhang Li [c], Lianwang Chen [a]

[a] Key Laboratory of Crustal Dynamics, Institute of Crustal Dynamics, China Earthquake Administration, Beijing 100085, China
[b] Department of Geological Science, University of Missouri, Columbia, MO 65211, USA
[c] Second Monitoring and Application Center, China Earthquake Administration, Xi'an 710054, China

ARTICLE INFO

Article history:
Received 7 March 2019
Received in revised form 3 July 2019
Accepted 9 July 2019
Available online 19 July 2019
Editor: A. Yin

Keywords:
southeastern Tibetan Plateau
strain partitioning
gravitational spreading
tectonic extrusion
numerical modeling

ABSTRACT

Crustal deformation in southeastern Tibetan Plateau has been attributed to tectonic extrusion and gravitational spreading. Here we analyzed the present-day strain partitioning in this region using GPS data. The results show highly localized shear strain along the Xianshuihe-Anninghe-Xiaojiang strike-slip faults, as expected by the model of tectonic extrusion. However, the localized shear strain along strike-slip faults ends in southern Yunnan and transfers to crustal extension in Yunnan and contraction in Myanmar. We developed three-dimensional visco-elastoplastic finite element models to investigate the causes of the observed crustal deformation. Our results indicate that the present-day crustal deformation in southeastern Tibetan Plateau can be largely explained by gravitational spreading.

1. Introduction

Southeastern Tibetan Plateau is one of the most tectonically and seismically active regions in the world (Fig. 1). The collision and continued convergence between the Indian and Eurasian plates in the past ~50 Ma have led to strong crustal deformation, rapid uplift, a complex system of large-scale strike-slip faults, and intense seismicity (Royden et al., 2008; Yin and Harrison, 2000). In the past century, more than forty $M \geq 6.7$ earthquakes occurred in this region.

Crustal deformation and seismicity in southeastern Tibetan Plateau provide key constraints for the competing models for the deformation and growth of the Tibetan Plateau. One is the tectonic extrusion model (Tapponnier et al., 1982), which states that the Indo-Asian collision is primarily accommodated by lateral translation of Asian lithospheric blocks along numerous large strike-slip faults (Leloup et al., 1995; Tapponnier et al., 1982). The well-developed large-scale strike-slip faults in southeastern Tibetan Plateau, including the Sagaing Fault, the Xianshuihe-Anninghe-Xiaojiang Fault and the Red River Fault that bound the northern part of the Indochina block (Fig. 1), and the large offsets across these faults, have been used to support this model.

Another model is gravitational spreading, in that crustal deformation in the Tibetan Plateau and surrounding regions is driven by the excess gravitational potential energy of the high plateau (England and Houseman, 1988; Flesch et al., 2001; Liu and Yang, 2003). England and Molnar (1997) showed that the strain rate field in the Tibetan Plateau and surrounding regions, derived from Quaternary fault slip rates, is consistent with viscous spreading driven by the gradient of gravitational potential energy.

Furthermore, lower crustal channel flow has been proposed to explain the large variations of topographic gradients in this region, including the sharp topographic slope across the eastern margin of the Tibetan Plateau and the gradational topography across southeastern Tibetan Plateau (Bischoff and Flesch, 2018; Clark and Royden, 2000). Some geophysical evidence has been reported to support this model (e.g., Bai et al., 2010; Burchfiel et al., 2008).

In the past decades extensive GPS measurements have been taken in southeastern Tibetan Plateau (e.g., Gan et al., 2007; Shen et al., 2005; Zhang et al., 2004; Zheng et al., 2017). These results show southward motion of the crust from the high plateau, with remarkable clockwise rotation around the eastern Himalayan syntaxis (Fig. 1). Whereas these results are sometimes regarded as indications of crustal extrusion from the Indian-Eurasian collision zone, detailed strain analysis is needed to understand the style and cause of crustal deformation.

In this paper, we first analyze the present-day strain rate field, focusing on strain partitioning and transfer, in southeastern Ti-

* Corresponding author at: 101 Geology Building, Department of Geological Sciences, University of Missouri-Columbia, MO 65211-1380, USA.
E-mail address: LiuM@missouri.edu (M. Liu).

https://doi.org/10.1016/j.epsl.2019.07.010
0012-821X/

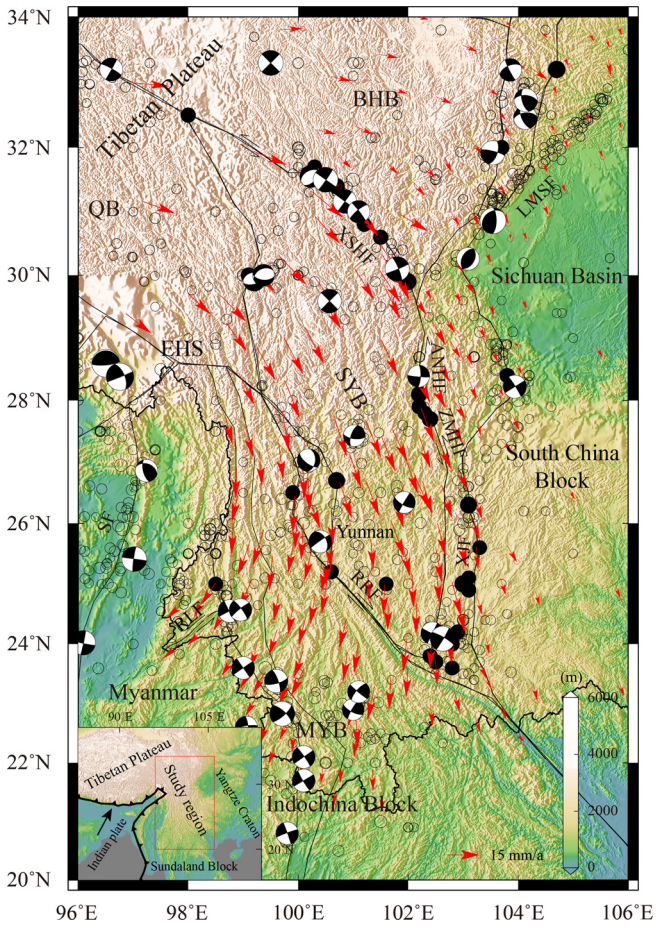

Fig. 1. Tectonic setting, topographic relief, GPS site velocities (red arrows, relative to stable Eurasia plate. Data source: (Wang, 2009)), and historic seismicity of the southeastern Tibetan Plateau. The black circles represent M ≥ 5.0 earthquakes since 1900, and the focal mechanisms of strong earthquakes (M ≥ 6.7) are shown; the black dots represent historic events of M ≥ 6.7 (source: Department of Earthquake Disaster Prevention, State Seismological Bureau, 1995, and Department of Earthquake Disaster Prevention, China Earthquake Administration, 1999). BHB: the Bayan Har block; EHS: Eastern Himalayan Syntaxis; MYB: the Myanmar-Yunnan block; QB: the Qiangtang block; SYB: the Sichuan-Yunnan block. XSHF: Xianshuihe Fault, ANHF: Anninghe Fault, ZMHF: Zemuhe Fault, XJF: Xiaojiang Fault, RRF: Red River Fault, LMSF: Longmen Shan Fault, RLF: Ruili-Longling Fault. (For interpretation of the colors in the figure(s), the reader is referred to the web version of this article.)

betan Plateau using the available GPS data. We then develop three-dimensional visco-elastoplastic finite element models to investigate the roles of tectonic extrusion and gravitational spreading in the present-day crustal deformation in southeastern Tibetan Plateau.

2. Tectonic background

Southeastern Tibetan Plateau is adjacent to the Yangtze craton to its east, the Indian-Burma plate to its west, and overlaps with the northern part of the Indochina block (Fig. 1). This part of the Tibetan Plateau consists of five major blocks with different geological structure and rheology, separated from each other by a complex system of faults (Zhang et al., 2003).

2.1. Main tectonic blocks

The northern part of southeastern Tibetan Plateau consists of the Bayan Har block and the eastern tip of the Qiangtang block. Seismic results suggest low velocities and high attenuation in the crust and upper mantle under both the Bayan Har and the Qiangtang blocks (Zhang et al., 2011). These two blocks in this region are regarded as the path for the southeastward exit of crustal material from the Indo-Eurasian collision zone.

Further south is the Myanmar-Yunnan block, which is located south of the east Himalayan syntaxis and accounts for the northern part of the Indochina block. Its western boundary is the Burma range subduction zone. The oblique subduction causes dextral motion along the Sagaing Fault.

In the central part of southeastern Tibetan Plateau is the Sichuan-Yunnan block, bounded by the strike-slip Xianshuihe-Xiaojiang fault system in the north and east, and the Red River Fault in the southwest. Geophysical results, including high heat flow, low resistivity, low velocity structure and seismic attenuation indicate a weak lower crust under this block. Shear-wave splitting data show that the fast polarization directions correlate well with the main strike-slip faults, topographic gradient, and geodetic estimate of the crustal strain (Lev et al., 2006), indicating vertically coherent south-southeastern motion of the crust and mantle from the collision zone (Wang et al., 2008). However, this coherence disappears in southern Yunnan, as the directions of fast polarization rotate nearly 90 degrees to become roughly E-W oriented (Gahalaut and Gahalaut, 2007; León Soto et al., 2012), and the GPS velocity vectors fan out (Fig. 1). The cause of this change remains uncertain.

The eastern side of southeastern Tibetan Plateau is bounded by the South China block, which has been tectonically and seismically stable with relatively low topographic relief (Burchfiel et al., 2008) and high seismic velocity in the lithosphere (Shen et al., 2003). This strong block has a significant influence on the Cenozoic deformation and strain distribution in southeastern Tibetan Plateau (Yin, 2010).

2.2. Major active faults

The study area has a complex system of active faults. The Longmen Shan Fault is the eastern boundary of the Tibetan Plateau. The GPS data indicates ~3 mm/a of convergence and ~1 mm/a of right-lateral slip along this fault (Burchfiel et al., 2008).

Major faults in southeastern Tibetan Plateau include the NW-SE trending Xianshuihe Fault and the nearly NS-trending Anninghe-Zemuhe-Xiaojiang faults (Fig. 1). These sinistral strike-slip fault zones facilitate the eastward and southeastward motion of the Tibetan crust (Wang et al., 1998). The Xianshuihe Fault is tectonically active; both geological and GPS measurements indicate 15 ± 5 mm/a left-lateral slip on its northwestern segments and 5-9 mm/a on its southeastern segments (Allen et al., 1991; Gan et al., 2007). Further south the Xianshuihe Fault connects with the Anninghe Fault, where the slip rate, based on geological and GPS data, is ~4.0 mm/a (Ran, 2008; Shen et al., 2005). Similar rates are reported for the Zemuhe Fault further south. The Xiaojiang Fault defines the southern part of the eastern boundary of the Sichuan-Yunnan block. The estimated late Quaternary strike-slip rate is 14-22 mm/a (He and Oguchi, 2008), while the geodetic slip rate is 7 ± 2 mm/a (Shen et al., 2005).

The Red River Fault, separating the South China block from the Indochina block, has long been recognized as a profound structure. Some studies suggested more than 700 km left-lateral offset on the Red River Fault during the Oligo-Miocene period (Leloup et al., 1995), providing key evidence for the tectonic extrusion hypothesis. However, some geological evidence used to infer such offsets has been questioned (Searle, 2006). During Miocene-Pliocene, the Red River Fault switched to right-lateral slip and the average slip rates is ~1.1 mm/a (Leloup et al., 2007; Shi et al., 2018a), with moderate to low level of historical seismicity.

Within the Myanmar-Yunnan block is a system of NE-SW trending secondary faults, along which the present-day clockwise crustal

rotation occurs (Shi et al., 2018b), as indicated by the GPS vectors (Fig. 1).

3. Stain rates and strain partitioning

In this section, we use the available GPS data to analyze the strain rates and strain partitioning in southeastern Tibetan Plateau. Extensive GPS measurements in southeastern Tibetan Plateau have been made in the last few decades (Gan et al., 2007; Wang, 2009). An update of the velocity field was obtained by combining the GPS data collected during 1991-2015 (Zheng et al., 2017), but the data is influenced by the 2008 Wenchuan earthquake (Mw 7.9). For this study, we use the GPS velocities in southeastern Tibetan Plateau based on the measurements during 1999-2007 by the Crustal Movement Observation Network of China (Wang, 2009) (Fig. 1).

Because of the uneven coverage of the GPS stations, we used the spherical wavelet-based multiscale approach (Tape et al., 2009) to derive spatially continuous velocity and strain rate fields. This method, based on weighted and damped least squares approach, automatically matches the local station density through a user-defined spherical grids of orders (q). Short-scale spherical wavelets are used where stations are dense. This method reduces the uncertainty from uniform interpolation algorithms. In this study, we used allowable grids for orders of q = 3-7, based on the GPS station coverage. Because the spherical wavelets are analytically differentiable, spatial gradient tensors such as strain rates, dilatation rates, and rotation rates can be directly computed (Tape et al., 2009).

We first calculated the horizontal velocity field in southeastern Tibetan Plateau. The magnitude of horizontal velocity is the highest around the Tibetan Plateau and gradually decreases southeastward (Fig. 2a).

Shear strain is concentrated along the Xianshuihe-Anninghe-Xiaojiang fault system (Fig. 2b). This is consistent with the high slip rates on these boundary faults. The highly concentrated shear strain along strike-slip faults is an essential feature of the tectonic extrusion model (Avouac and Tapponnier, 1993; Tapponnier et al., 1982). However, the localized shear strain does not extend to the Red River Fault and beyond, as would be expected in the extrusion model. Instead, the shear strain terminates in southern Yunnan and transfers to crustal contraction in Myanmar and extension in Yunnan. Some elevated shear strain is found in northern Myanmar-Yunnan block, associated with the system of subparallel NE-SW trending strike-slip faults, which accommodates the clockwise crustal rotation (Fig. 2a). On the other hand, the Longmen Shan Fault shows relative low shear strain, owing to the crust motion roughly perpendicular to the fault strike. This is consistent with the high-angle thrusting in southern Longmen Shan Fault as shown by the 2008 Wenchuan and 2013 Lushan earthquakes (Xu et al., 2013; Zhang et al., 2010). The Red River Fault also has a low shear strain, consistent with its low strike-slip rate and sparse seismicity (Shi et al., 2018a; Yin et al., 2018).

Near the southern end of the Xianshuihe-Anninghe-Xiaojiang fault system, the high shear strain ends and transfers to contraction and dilatation (Fig. 2c). Dilatation in southern Yunnan is part of the overall extension in the Sichuan-Yunnan block (SYB), as indicated by the fan-shaped divergence of crustal motion (Fig. 2a). Further to the west, this crustal motion is resisted by the MYB, explaining the compressive strain there (Fig. 2c). Another region of high compressive strain is along the southern segment of the Longmen Shan Fault (Fig. 2c), indicating significant convergence between the eastern Tibetan Plateau and the strong Sichuan Basin (Burchfiel et al., 2008). Consistent with extrusion along the Xianshuihe-Anninghe-Xiaojiang fault system is the high rotational rate (Fig. 2d). The rigid crustal blocks have to rotate as the strike of the fault system, hence the crustal motion along it, changes from NW-SE in the north to nearly N-S in the south.

These results of strain rates show that crustal extrusion along major strike-slip faults ends in southern Yunnan and transfers to crustal contraction and dilatation.

4. The finite element model

We developed three-dimensional visco-elastoplastic finite element models to explore the relative roles of gravitational buoyancy force and the lateral driving force from the Indo-Asian collision in causing the observed present-day crustal deformation in southeastern Tibetan Plateau (Fig. 3). The model incorporates the topographic relief, faults bounding the major blocks (represented by a 10-km thick weak zone), and the first-order variation of physical property between the strong South China block and the rest of the blocks in the study region. To minimize artificial boundary effects, the model domain spans a large region (Fig. 3), and the bottom of the model domain is at 90 km depth. The model is composed of eight-node hexahedral elements, consists of 14,691 elements with 22,540 active nodes.

We first use separated models to illustrate the effects of gravitational spreading and tectonic extrusion. To simulate the strain rates caused by gravitational spreading, we assume the generalized Maxwell viscoelastic rheology (the Prony series) for the model domain. The model includes a stiffer South China block, whose effective viscosity is taken to be 4×10^{21} Pa s for the upper crust and 8×10^{22} Pa s for the lower crust and upper mantle. For the rest of the region, we used 8×10^{20} Pa s for the upper crust and 4×10^{22} Pa s for the rest of the lithosphere (Flesch et al., 2001; Shi and Cao, 2008). The Young's modulus and Poisson's ratio used in the model are 8.0×10^{10} Pa and 0.26, respectively; the density of the crust and upper mantle are taken to be 2800 and 3300 kg m^{-3}, respectively. The lateral boundaries are fixed in the normal direction. The top surface is free; the bottom is free-slip in the horizontal direction and fixed in the vertical direction. We hereafter refer to this model as the reference model.

The model simulates crustal deformation by solving the general equation of force balance,

$$\frac{\partial \sigma_{ij}}{\partial x_j} + \rho g_i = 0 \tag{1}$$

where σ_{ij} is the stress tensor ($i, j = 1, 2, 3$), ρ is the density and g is the gravitational acceleration.

In viscoelasticity, stress relates to strain rate and depends on the stress-strain history, so a hereditary integral is used,

$$\sigma = 2\int_0^t G(t-\tau)\frac{de}{d\tau}d\tau + I\int_0^t K(t-\tau)\frac{d\Delta}{d\tau}d\tau \tag{2}$$

where σ is the Cauchy stress, e is deviatoric strain, Δ is volumetric strain, τ is past time, and I is the identity tensor. $G(t)$ and $K(t)$ are the Prony series shear and bulk-relaxation modulus, respectively:

$$\begin{cases} G(t) = G_\infty + \sum_{i=1}^{n_G} G_i \exp\left(-\frac{t}{\tau_i^G}\right) \\ K(t) = K_\infty + \sum_{i=1}^{n_K} K_i \exp\left(-\frac{t}{\tau_i^K}\right) \end{cases} \tag{3}$$

where τ_i^G is the relaxation time for each Prony component G and depends on viscosity. G_i is the shear modulus of the ith Prony unit whereas G_∞ is the long-term modulus ($t = \infty$), and n_G is the

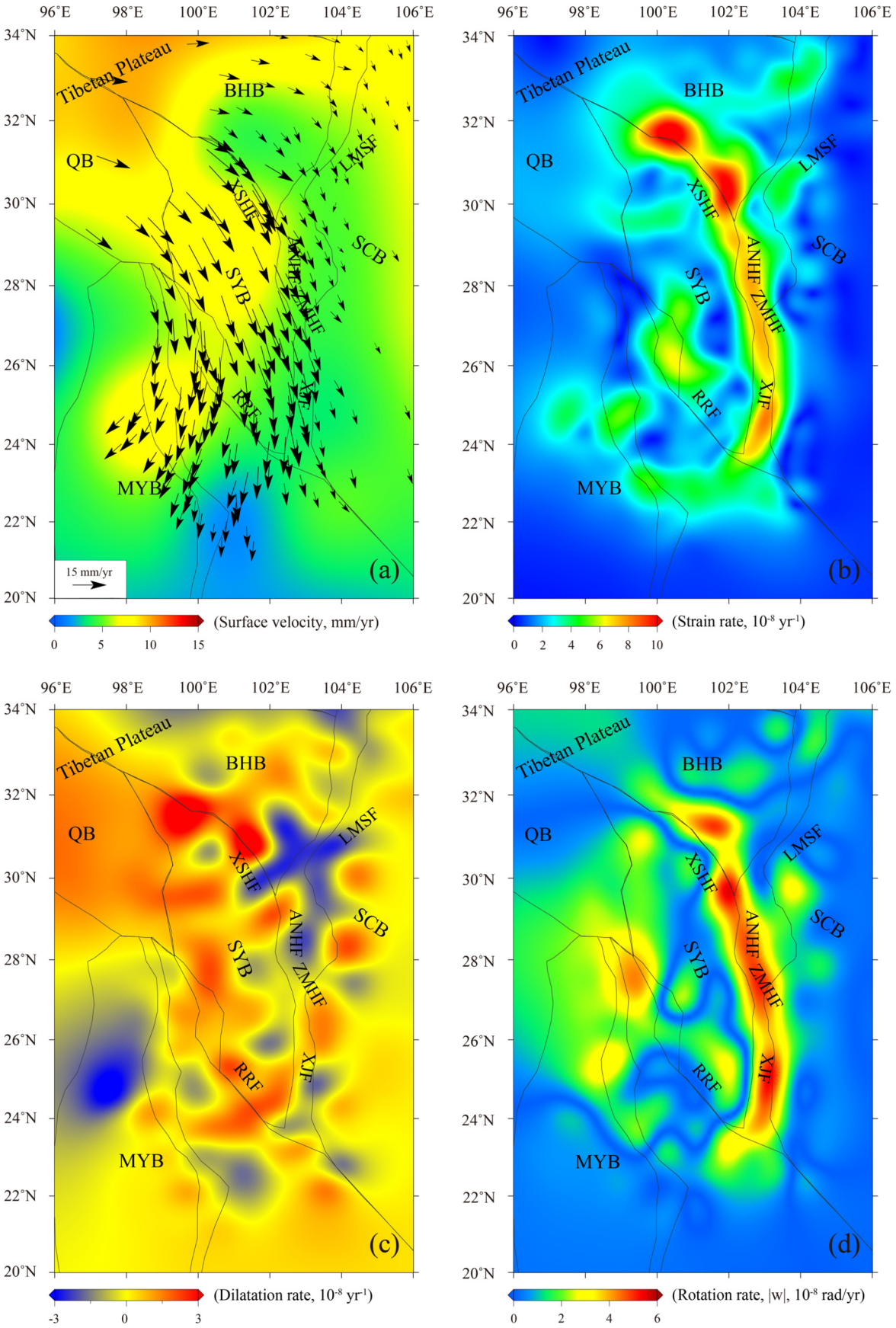

Fig. 2. Surface velocity and horizontal strain rate fields in southeastern Tibetan Plateau. The black lines are boundaries of tectonic blocks. The abbreviations for blocks and faults are explained in Fig. 1. (a) GPS velocity field (arrows). The background color contours show the magnitude of the horizontal velocity. (b) The maximum shear strain rate; (c) Dilatation strain rate, negative for compressive; (d) Magnitude of rotational strain rate.

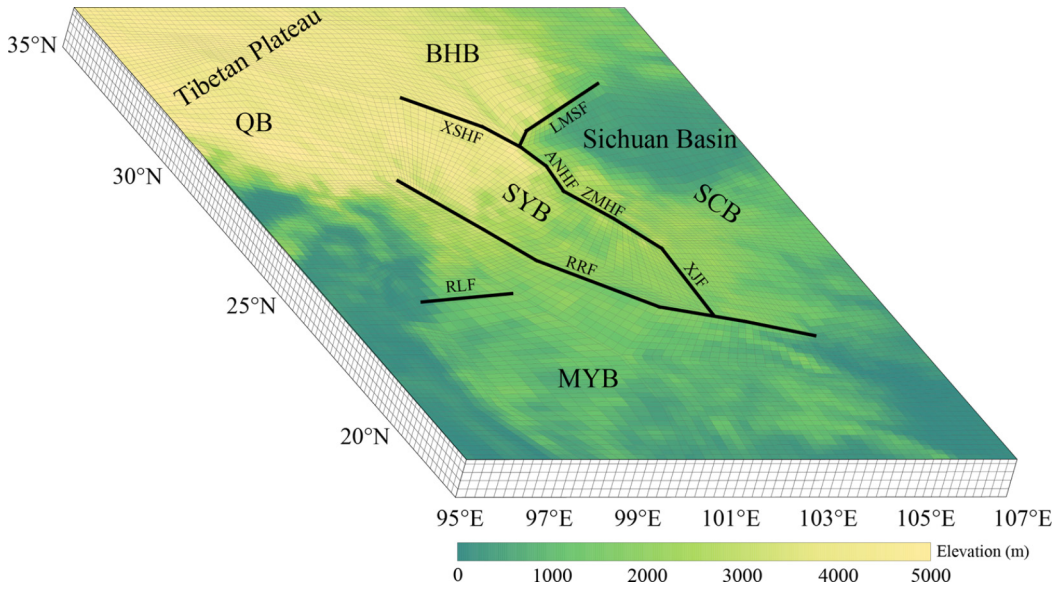

Fig. 3. Three-dimensional visco-elastoplastic finite element model of southeastern Tibetan Plateau. The black lines represent the major faults included in the model; the abbreviations are explained in Fig. 1.

number of Prony terms. Similar behavior can be defined for bulk relaxation modulus $K(t)$ with a separate set of n_K values of Prony terms.

When we simulate tectonic extrusion as suggested in the analogue plasticine model by Tapponnier et al. (1982), we assume elastoplastic rheology for the model. Different plastic yielding strength are assigned to the South China block (2.0×10^7 Pa) and the other blocks (1.5×10^7 Pa), and a lower value for the fault zones (5.0×10^6 Pa). The plasticity is expressed as the Bilinear Kinematic Hardening Plasticity model (Luo and Liu, 2010), in which the stress-strain ratio follows Young's modulus before the yielding point. In these models, we imposed a velocity boundary (20 mm/a) on the northern and northwestern sides of the model domain, based on the GPS data, to simulate the lateral tectonic force that drives tectonic extrusion. The eastern boundary is a pulley-like boundary, simulating obstruction by the South China block; the bottom is free-slip in the horizontal direction and fixed in the vertical direction, and the other sides are free.

All modeling was conducted using the ANSYS® finite element software. ANSYS® employs the Newton-Raphson approach to solve nonlinear problems. In this method, a load is subdivided into a series of increments applied over several steps. Prior to each solution, the out-of-balance load vector is evaluated. If the convergence criteria are not satisfied, the load vector is reevaluated, the stiffness matrix updated, and a new solution is obtained until convergence is reached.

5. Model results

5.1. The effects of gravitational spreading

Fig. 4 shows the results of crustal motion driven by gravitational spreading. In this reference model, all sides of the model domain are fixed, so the crustal deformation is entirely caused by topographic loading in the study area. The predicted surface motion is close to the GPS velocity field. The residual velocity vectors are mostly <5 mm/a (Fig. 4b). The directional difference between the GPS and the predicted velocities are mostly $<15°$. Misfits are mainly found in two regions; both can be attributed to the fixed boundary conditions of this model. One is the northwestern corner of the study area, where the SE motion of the Tibetan crust into the study region is not included in the model. Another is near the southwestern side of the study area, where the fixed boundary does not help reproducing the clockwise rotation of the GPS velocity vectors.

This reference model of gravitational spreading can be improved by including other factors. First, as a first-order approximation, we included the major boundary faults (as 10-km wide weak zones with half of the viscosity value as the surrounding crust) in the model. Their main effects are to increase the southward crustal motion because of the approximately north-south strikes of these faults and the topographic gradients in this direction. This improves fitting to the GPS data, mainly near the faults and in the southern part of the study area.

The fixed boundary condition (zero velocity) imposed on all sides of the model domain is clearly an oversimplification. Replacing it with a free boundary on the southwestern side (roughly south of 25°N), where southwestward crustal motion may be facilitated by the subduction zone further to the west (Gahalaut and Gahalaut, 2007), significantly improves the fitting by allowing the clockwise rotation in the western Yunnan region as observed in the GPS data (Fig. S1).

The simplification of faults in the model also contributes to the misfit. The kinematic analysis by Shi et al. (2018a, 2018b) suggests that the clockwise rotation of the Myanmar-Yunnan region is closely associated with a fan-shaped system of sinistral strike-slip faults. We tested this by including the simplified NE-trending Ruili-Longling Fault in the model, and found slightly enhanced clockwise rotations in this region that improve fitting to the GPS velocity field. Further improvement is gained by assuming a weaker lower crust in the northwestern part of the Sichuan-Yunnan block (Fig. S2), where low seismic velocity and low electrical resistivity are reported.

Fig. 5 shows the results of the preferred model that includes all the aforementioned improvements. The misfits of surface velocity are reduced (cf. Fig. 4b), especially in the Myanmar-Yunnan region (Fig. 5a), and the predicted strain rate pattern (Fig. 5b) is generally comparable with that derived from the GPS data (Fig. 2). These results indicate that the observed present-day crustal motion in southeastern Tibetan Plateau can be largely explained by gravitational spreading.

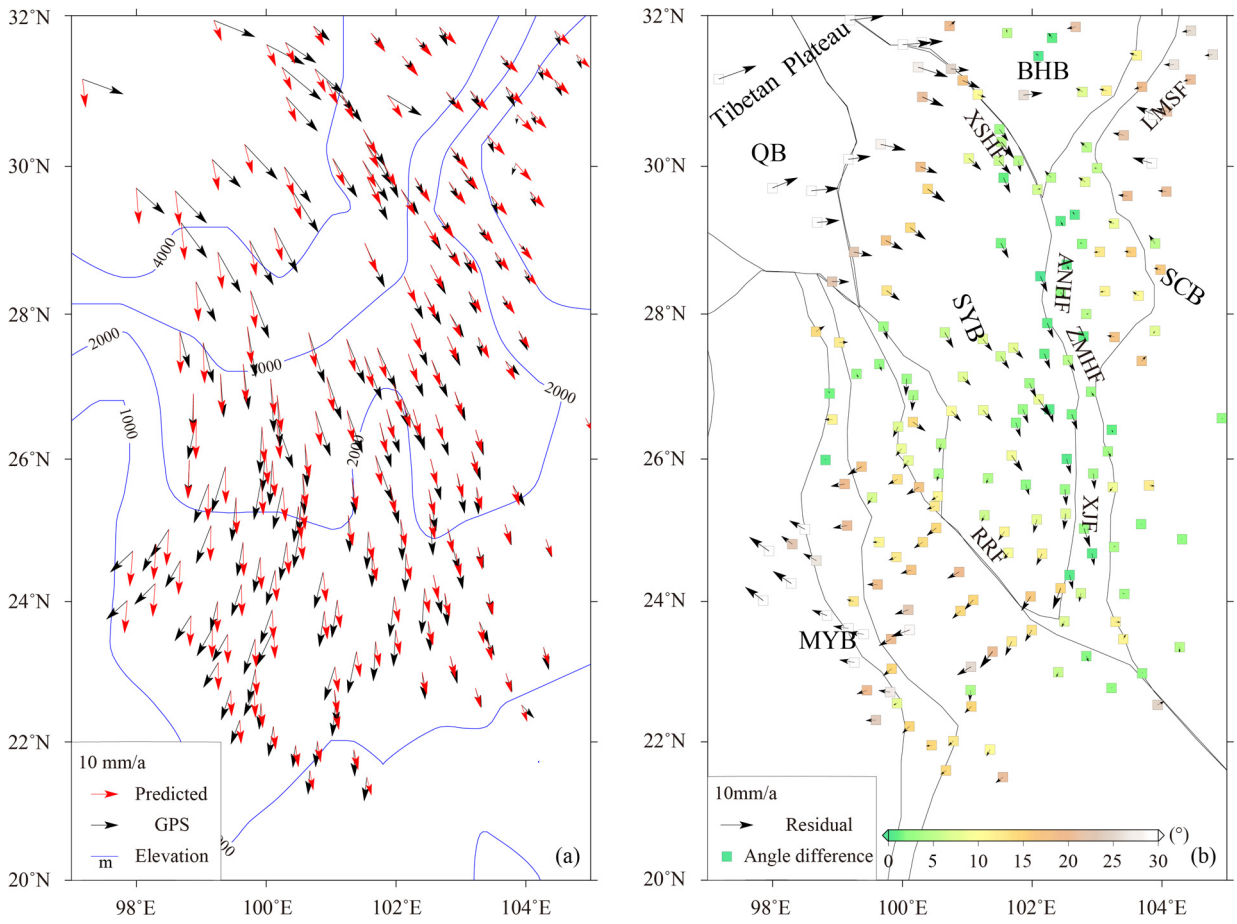

Fig. 4. (a) Comparison of the GPS velocities with the predicted surface velocity by the reference model of gravitational spreading. Blue lines are topographic contours. (b) The residuals of the magnitude and direction (shown in color of each arrow) between the predicted and the GPS velocities.

5.2. The tectonic extrusion model

We then explored whether or not the observed present-day crustal deformation in southeastern Tibetan Plateau can be alternatively explained by tectonic extrusion of lithospheric blocks along major strike-slip faults. To simulate tectonic extrusion, the model assumes a flat lithosphere with major strike-slip faults in this region, and the key model parameters were discussed in section 4. The lateral driving force from the Indo-Asian collision is simulated by imposing a 20 mm/a velocity on the northern and northwestern edges of the model domain (Fig. 6a). The model starts with arbitrary initial stress (zero MPa). After being loaded for about 50 Ka, the model reaches a quasi-steady state. Further loading is accommodated by steady-state plastic creeping along the faults, with nearly constant stresses and strain rates in the model.

The results show improved fitting of the surface crustal velocity to the GPS data in the northwestern part of the study area (Fig. 6a) relative to the gravitational spreading model, largely because of the imposed boundary velocity in this case. The fit in the rest part of the region, however, is poor. In the tectonic extrusion model, lithospheric blocks move coherently along strike-slip faults, hence the rather uniform southward crustal motion in the model. The model does not reproduce the intra-block strain or the clockwise crustal rotation in the Myanmar-Yunnan region (Fig. 6a).

To explore the effects of the boundary conditions on the model results, we replaced the free-sliding (pulley-like elements) boundaries on the eastern side with a free boundary (Fig. S3) or with a velocity boundary based on the GPS data in the boundary regions (Fig. S4). The effects are insignificant. This is because the extrusion model assumes sliding of rigid lithospheric blocks along strike-slip faults; hence crustal motion is largely controlled by the orientation and strength of these faults, and not sensitive to the far-field boundary conditions.

The resulting strain rate pattern (Fig. 6b) differs significantly from that derived from the GPS data (Fig. 2b). The predicted high shear strain in the northwestern part of the model domain results from the imposed velocity boundary condition. The shear strain is localized along the main strike-slip faults, as expected, but it dies out in the southern part of the model domain, because the crust moves as rigid blocks with little internal deformation (Fig. 6b). Reducing the yielding strength of the fault zones causes higher strain concentration along the faults, but the spatial pattern of strain rates remains the same. We have explored the model parameters and found that it is difficult for the tectonic extrusion model to explain the present-day crustal deformation in southeastern Tibetan Plateau.

5.3. Results of a combined model

We have shown that the model of gravitational spreading could explain most of the GPS data in southeastern Tibetan Plateau except in the northwestern part of the study area, where the misfit is significantly reduced in the tectonic extrusion model. We constructed a model that includes lateral boundary-push in the tectonic extrusion model (Fig. 6) to the optimal gravitational spreading model (Fig. 5). The results are better fits to the GPS data than either the gravitational spreading model or the tectonic extrusion model alone. The combined model captures the main features of the GPS velocity field, including the clockwise rotation in the Myanmar-Yunnan region (Fig. 7a). Adding the velocity boundary

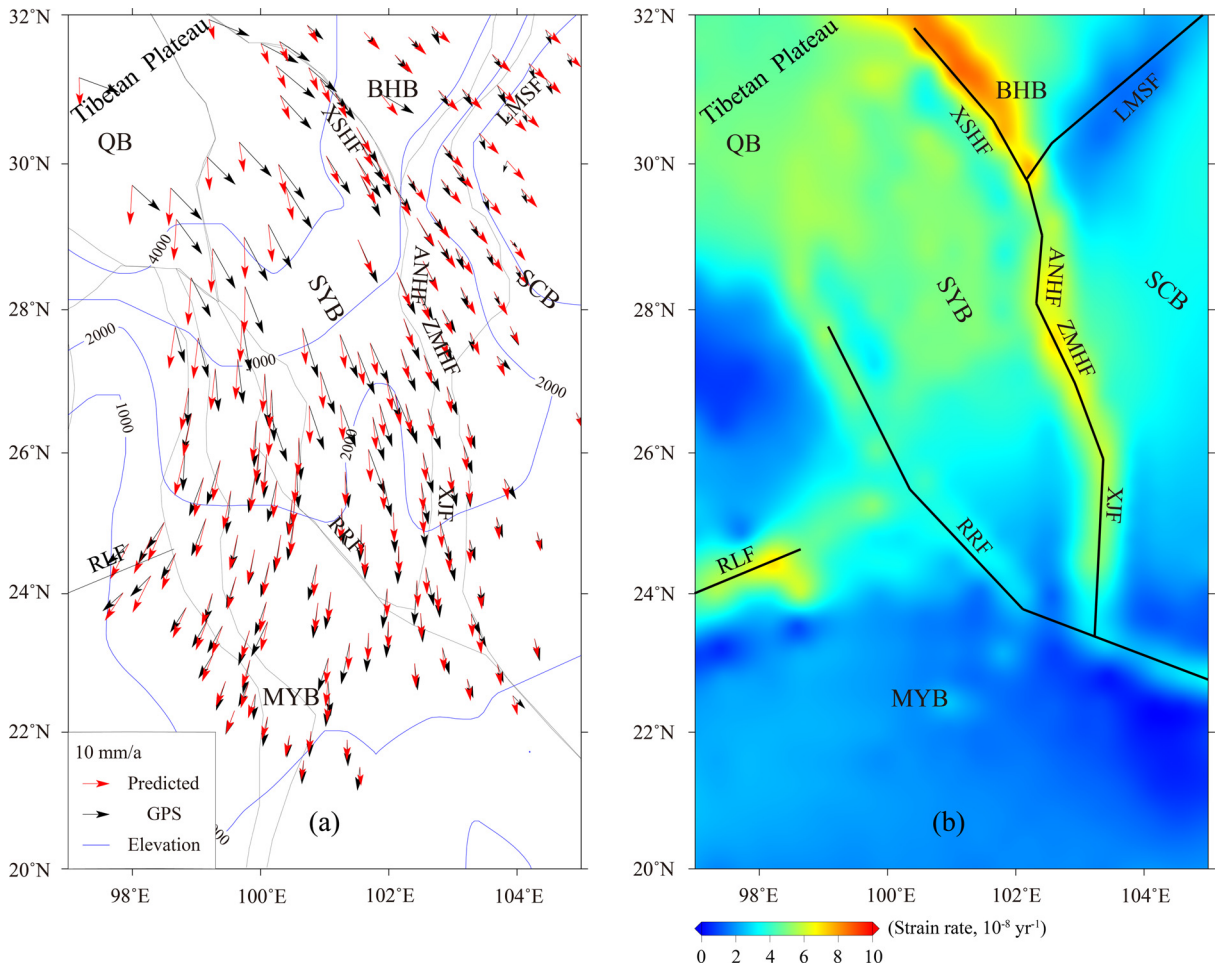

Fig. 5. Results of the preferred model of gravitational spreading. (a) Comparison of the GPS velocities with the predicted surface velocity. (b) The predicted maximum shear strain rates. Black lines are the major faults included in the model.

condition on the northwestern corner of the study area, generally regarded as the pathway for the eastward extrusion of Tibetan Plateau, significantly improve fitting to the GPS velocity in this area. The shear strain rates predicted by this optimal model also compare well with those derived from the GPS data, which are highly localized along the Xianshuihe-Xiaojiang fault system but gradually terminate in southern Yunnan (Fig. 7b).

6. Discussion

We have analyzed the available GPS data for present-day crustal deformation in southeastern Tibetan Plateau, and explored the causes of the observed crustal deformation in finite element geodynamic models. The results are helpful for understanding the crustal kinematics and dynamics in this region.

6.1. Strain partitioning and transfer

The GPS site velocities in southeastern Tibetan Plateau, with its impressive clockwise rotation around the eastern Himalayan syntaxis (Fig. 1), are often used to show the extrusion, or outward flow, of the Tibetan crust from the Indo-Asian collision zone. The GPS velocity vectors, however, change with the chosen reference frame. Analysis of strain rates, which are determined by the distribution and gradients of the velocity field and independent of its reference frame, is needed to understand crustal deformation measured by the GPS data. Using the wavelet-based multiple scale method (Tape et al., 2009), we analyzed strain rates in southeastern Tibetan Plateau. This method is based on the GPS velocity and makes no assumptions of the actual faults. The results show highly localized shear strain along the major strike-slip faults, especially the Xianshuihe-Anninghe-Xiaojiang fault system (Fig. 2b). This is consistent with the tectonic extrusion model that predicts rigid lithospheric blocks moving away from the Indo-Asian collision zone along the system of strike-slip faults within and around the Tibetan Plateau (Avouac and Tapponnier, 1993; Tapponnier et al., 1982). However, our results suggest that such tectonic extrusion is largely limited within the Tibetan Plateau. The localized shear strain does not extend to the Red River Fault and beyond; it essentially ends in southern Yunnan and transfers to crustal contraction and extension (Fig. 2c).

Our results of strain rates are consistent with previous studies of geological and contemporary geodetic slip rates along the major faults in this region, including high slip rates (5-20 mm/a) along the Xianshuihe-Anninghe-Xiaojiang fault system and low slip rate (2-5 mm/a) on the Red River Fault (Wang et al., 1998; Zheng et al., 2017). These results are also consistent with seismicity in southeastern Tibetan Plateau. In the past ~500 years, clusters of large earthquakes ($M \geq 6.5$) occurred along the Xianshuihe-Anninghe-Xiaojiang fault system, but earthquakes on the Red River Fault has been minimal (Yin et al., 2018), especially on the middle segment that shows lower shear strain rate and high dilatation rate. The high contraction rate along the Longmen Shan Fault zone is consistent with strong crustal compression there and the high-angle thrust faulting demonstrated by the 2008 Mw 7.8 Wenchuan earthquake (Burchfiel et al., 2008).

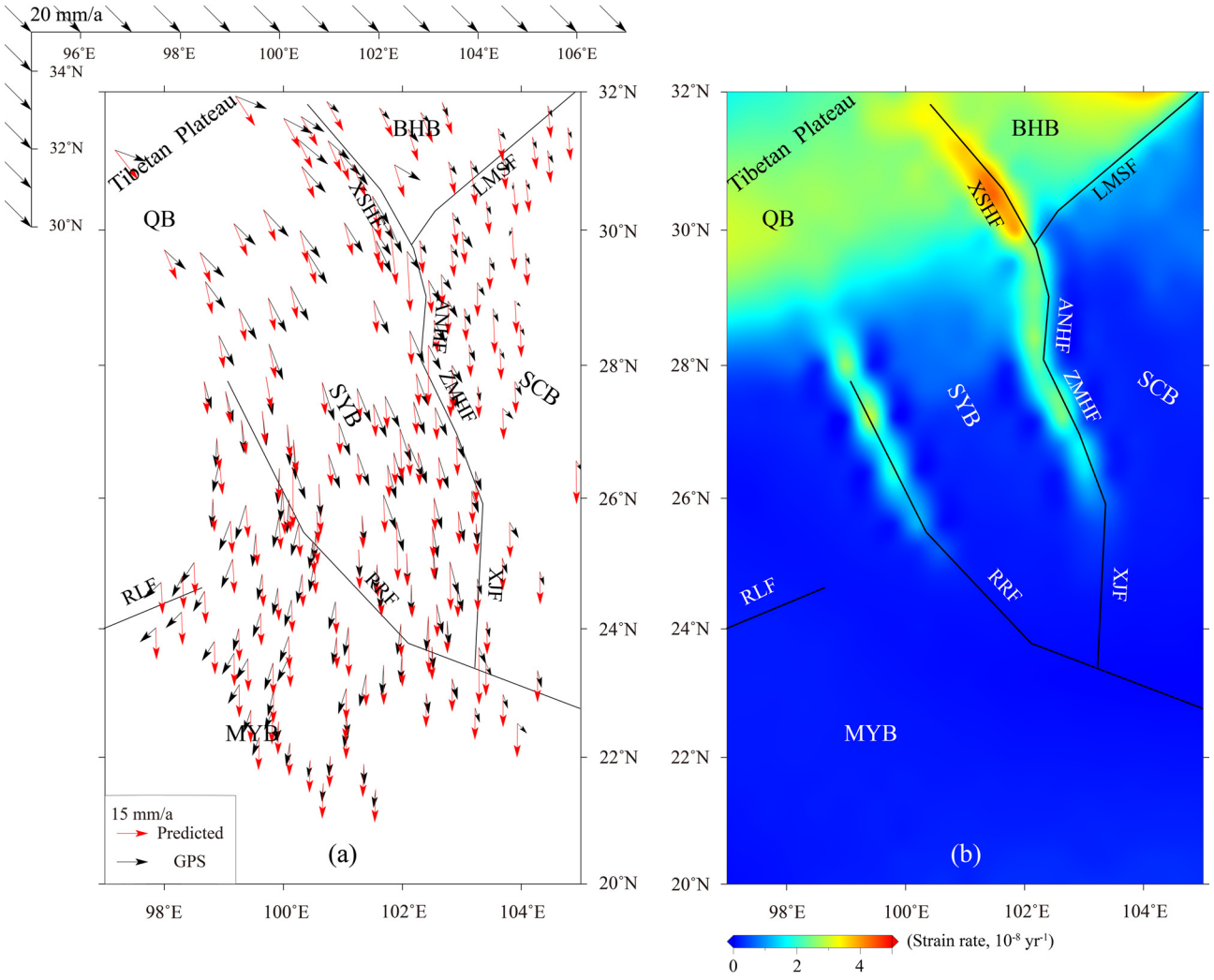

Fig. 6. Results of the tectonic extrusion model. (a) Comparison of the GPS velocities with the predicted surface velocity. Black lines are the major faults included in the model. The uniform black arrows show the imposed velocity boundary condition to simulate the lateral driving force. (b) The predicted maximum shear strain rate.

6.2. The cause of the present-day crustal deformation

Crustal deformation in southeastern Tibetan Plateau has been attributed to gravitational spreading (England and Houseman, 1988), lower crustal flow (Bischoff and Flesch, 2018; Clark and Royden, 2000), and tectonic extrusion (Tapponnier et al., 1982). We developed a set of simple forward models to investigate the basic roles of these mechanisms. Our results suggest that present-day crustal deformation in southeastern Tibetan Plateau can be largely explained by gravitational spreading. Similar conclusion has been reached by England and Molnar (1997) based on Quaternary fault slip rates in the Tibetan Plateau and surrounding regions, and by Flesch et al. (2001), Liu and Yang (2003), and Yang and Liu (2013) based on large-scale geodynamic modeling.

The dominant role of gravitational spreading in the present-day crustal deformation can be seen directly from the directions of the GPS velocity vectors (relative to stable Eurasia plate), which are approximately parallel to the topographic gradients (i.e., orthogonal to the topographic contours as shown in Fig. 4a). More supporting evidence includes the principal compressive stress axes, obtained from in-situ stress measurements and focal mechanism solutions, which are subparallel to the topographic gradient (Hu et al., 2017).

The lower crust flow model is similar to the gravitational spreading model when the pressure gradient that drives the low crustal flow arises from the topographic gradient. Some geophysical results suggest the existence of partial melt and low viscosity in the mid-lower crust under the Sichuan-Yunnan region (Bao et al., 2015; Liu et al., 2014). Our models do not directly test the channel flow model, but we found slight improvement of fitting to the GPS velocities when a low-viscosity lower crust is included in our geodynamic model (Fig. S2).

Our optimal model requires imposing southeastward velocities on the northwestern corner of the model domain (Fig. 7), which may represent outward gravitational spreading of the Tibetan Plateau, or the lateral tectonic driving force from the Indo-Asian collision as depicted in the tectonic extrusion model (Tapponnier et al., 1982). However, we have found that this lateral push alone cannot explain the observed present-day crustal deformation in southeastern Tibetan Plateau, because sliding of nearly rigid lithospheric blocks along the strike-slip fault cannot explain the internal strain in each block as shown by the GPS data.

Of course, some blame can be placed on the oversimplification of the fault systems in our model. Many secondary faults are not included, especially the fan-shaped distribution of a system of sinistral faults in Myanmar-Yunnan region (Shi et al., 2018b), which could improve the model fitting by producing distributed clockwise rotation in this region.

Whereas the overall fitting may be further improved by including more complexities, such as secondary faults and lateral variations of lithospheric viscosity, in the model, the purpose of

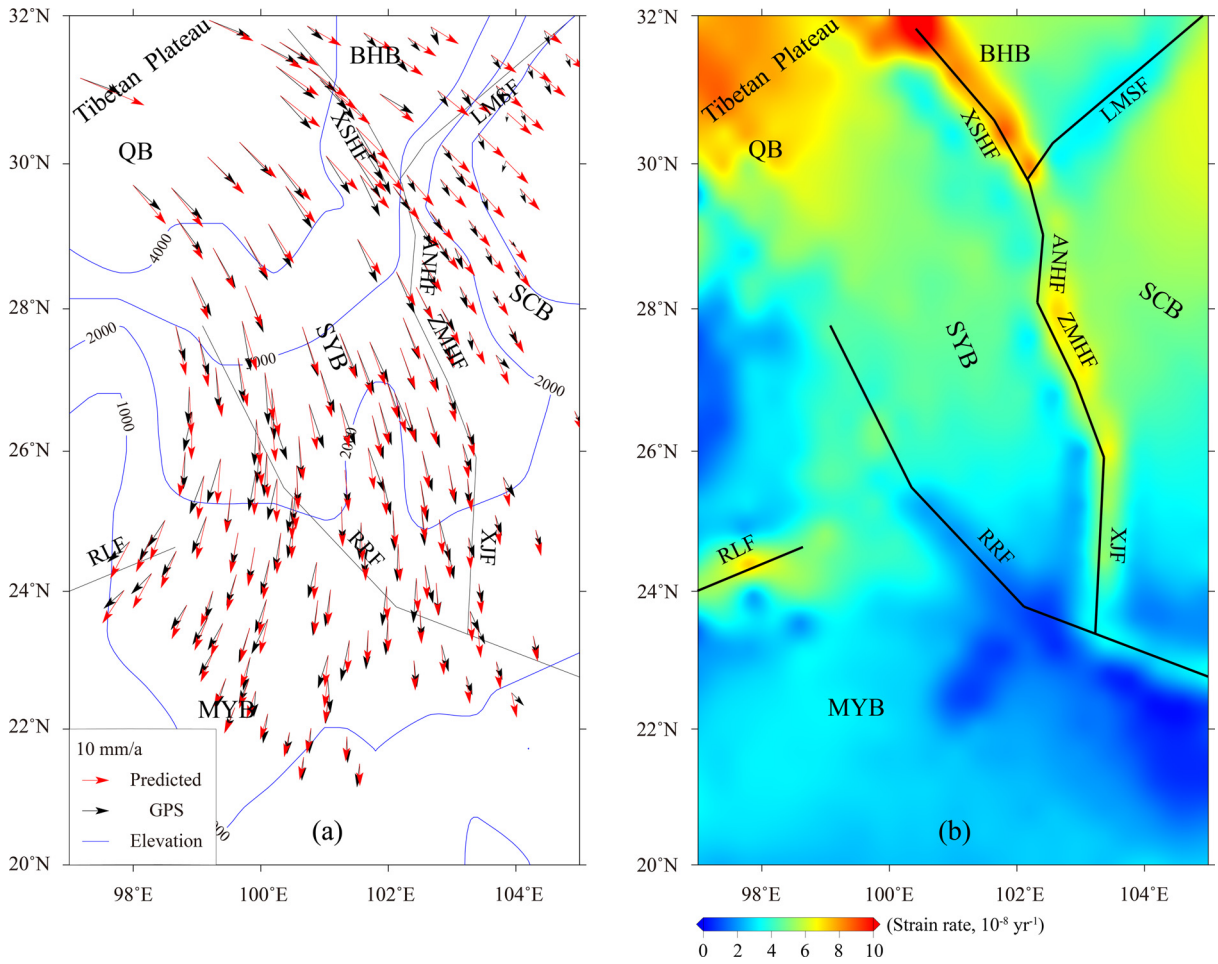

Fig. 7. Results of the model combining gravitational spreading and tectonic extrusion. (a) Comparison of the GPS velocities with the predicted surface velocity. (b) The predicted maximum shear strain rate.

our geodynamic models is not to fit the details of observations but to illustrate the fundamental physics controlling the crustal deformation. That the overall strain rates pattern can be largely explained by the simple model of gravitational spreading indicates the dominant role of gravitational potential energy in driving the present-day crustal deformation, and the termination of fault-localized shear strain in southern Yunnan means that significant tectonic extrusion does not extend beyond the margin of the Tibetan Plateau.

6.3. Tectonic implications

It is well known that the Indo-Eurasian continental collision in the past ~50 Ma has raised the Himalayan Tibetan Plateau, but its impact on other part of Asian continent has been less clear. The viscous thin-sheet model (England and McKenzie, 1982), which approximates the Asian continent as a viscous thin sheet and simulates the collisional process in continuum mechanics, suggests that the collision and the resulting crustal shortening are largely accommodated by crustal thickening (England and Houseman, 1988). In this case, the tectonic impact of the Indo-Eurasian collision would be largely limited to the Himalayan–Tibetan Plateau and surrounding regions. On the other hand, the tectonic extrusion (escaping) model predicts the Indo-Eurasian collision to cause large-scale eastward and southeastward translation of lithospheric blocks along major strike-slip faults (Tapponnier et al., 1982). In this model, the Indo-Eurasian collision would control Cenozoic tectonics in much of Central and East Asia. Large offsets and high slip rates on the strike-slip faults within and around the Tibetan Plateau, as well as highly localized strain on these faults, provide the major evidence for the tectonic extrusion model (Avouac and Tapponnier, 1993; Tapponnier and Molnar, 1977).

Southeastern Tibetan Plateau is the main exit for the extruding lithospheric blocks in the tectonic extrusion model (Tapponnier et al., 1982), hence an important place to test the competing models. Our strain rate analysis shows highly localized shear strain along the Xianshuihe-Anninghe-Xiaojiang fault system, which is consistent with the tectonic extrusion model. However, such fault-localized shear strain ends in southern Yunnan and transfers to crustal compression in Myanmar and extension in Yunnan. In other words, tectonic extrusion along the strike-slip faults is largely limited within the Tibetan Plateau. Similar conclusion has been reached by studies of strain rates in northeastern Tibetan Plateau, where strain localization along the major strike-slip faults ends and transfers to crustal compression and thickening near the eastern margin of the Tibetan Plateau (Li et al., 2018). Such strain transfer near the margins of the Tibetan Plateau provides the dynamic link between tectonic extrusion and crustal thickening and uplift in the Tibetan tectonics that has not been well established in previous models.

The results of terminating crustal extrusion near the margin of southeastern Tibetan Plateau are consistent with the decreasing slip rates along the Xianshuihe-Anninghe-Xiaojiang fault system (Zheng et al., 2017) and the minimal slip rates on the Red River Fault (Gan et al., 2007). They are also consistent with the geological reconstruction of crustal deformation that suggests lim-

ited extrusion in this region in the past 5 Ma (Replumaz and Tapponnier, 2003). These results, however, do not say anything directly about whether or not large-scale tectonic extrusion occurred in the geological past, because GPS data reflect only the present-day crustal deformation and much of the GPS-measured strain is elastic (Yang and Liu, 2010). Most extrusion models suggest that large amount extrusion in this region occurred during 15-30 Ma (Replumaz and Tapponnier, 2003), although some of the geological evidence used to infer such tectonic extrusion has been questioned (Searle, 2006). On the other hand, our geodynamic modeling suggests that present-day crustal deformation in southeastern Tibetan Plateau, including the localized shearing along the strike-slip faults, are mainly driven by the gravitational spreading of the uplifted Tibetan Plateau. Similar conclusions have reached by previous continental scale dynamic models (Flesch et al., 2001; Kong et al., 1997). Hence different factors, such as the change of tectonic boundary conditions, are needed to explain why the large scale tectonic extrusion does not occur today. Alternatively, the geological evidence for the large scale tectonic extrusion may also need reexamination.

7. Conclusions

We analyzed the strain rates field in southeastern Tibetan Plateau, and used three-dimensional finite element models to explore the causes of the observed crustal deformation. Major conclusions we may draw from this work including the following.

1) The GPS data show highly localized shear strain along the sinistral Xianshuihe-Anninghe-Xiaojiang fault system, consistent with tectonic extrusion along these faults. However, such tectonic extrusion ends in southern Yunnan and transfers to crustal extension and contraction. Thus the present-day tectonic extrusion along large-scale strike-slip faults occurs mainly within the Tibetan Plateau and transfers to crustal compression, and in some places extension, near the plateau's margins.

2) The present-day crustal deformation in southeastern Tibetan Plateau can be largely explained by gravitational spreading. Southeastward crustal motion around the eastern Himalayan syntaxis, either from gravitational spreading of the Tibetan Plateau or from collision-induced lateral tectonic driving force, is needed to explain the strain rates in the northwestern part of the study area, and rheological weak fault zones are needed to account for the localized shear strain. On the other hand, edge-push alone, as depicted in the tectonic extrusion model, cannot explain the observed strain rate partitioning and strain transfer in southeastern Tibetan Plateau.

Acknowledgements

We are grateful to three anonymous reviewers for their constructive comments. This work was performed during Y. Li's visit to the University of Missouri, supported by the China Scholarship Council. Research support was provided by the National Natural Science Foundation of China (grants 41874116, 41774111, and 41774107), the Research Grant from Institute of Crustal Dynamics, China Earthquake Administration (No. ZDJ2017-07), and the China Earthquake Science Experiment Project (No. 20150115). We are grateful to Wang Min for providing the GPS data. Most figures in the paper are plotted by GMT (Wessel et al., 2013).

Appendix A. Supplementary material

Supplementary material related to this article can be found online at https://doi.org/10.1016/j.epsl.2019.07.010.

References

Allen, C.R., Luo, Z.L., Qian, H., Wen, X.Z., Zhou, H.W., Huang, W.S., 1991. Field study of a highly active fault zone: the Xianshuihe fault of southwestern China. Geol. Soc. Am. Bull. 103, 1178–1199.
Avouac, J.P., Tapponnier, P., 1993. Kinematic model of active deformation in central Asia. Geophys. Res. Lett. 20, 895–898.
Bai, D., Unsworth, M.J., Meju, M.A., Ma, X., Teng, J., Kong, X., Sun, Y., Sun, J., Wang, L., Jiang, C., 2010. Crustal deformation of the eastern Tibetan plateau revealed by magnetotelluric imaging. Nat. Geosci. 3, 358–362.
Bao, X., Sun, X., Xu, M., Eaton, D.W., Song, X., Wang, L., Ding, Z., Mi, N., Li, H., Yu, D., 2015. Two crustal low-velocity channels beneath SE Tibet revealed by joint inversion of Rayleigh wave dispersion and receiver functions. Earth Planet. Sci. Lett. 415, 16–24.
Bischoff, S.H., Flesch, L.M., 2018. Normal faulting and viscous buckling in the Tibetan Plateau induced by a weak lower crust. Nat. Commun. 9, 4952.
Burchfiel, B.C., Royden, L.H., Van der Hilst, R.D., Hager, B.H., Chen, Z., King, R.W., Li, C., Lu, J., Yao, H.J., Kirby, E., 2008. A geological and geophysical context for the Wenchuan earthquake of 12 May 2008, Sichuan, People's Republic of China. GSA Today 18, 5.
Clark, M.K., Royden, L.H., 2000. Topographic ooze: building the eastern margin of Tibet by lower crustal flow. Geology 28, 703–706.
Department of Earthquake Disaster Prevention, State Seismological Bureau, 1995. The Catalogue of Chinese Historical Strong Earthquakes. Seismological Press, Beijing, pp. 1–529.
Department of Earthquake Disaster Prevention, China Earthquake Administration, 1999. The Catalogue of Chinese Modern Earthquakes. China Science and Technology Press, Beijing, pp. 1–637.
England, P., McKenzie, D., 1982. A thin viscous sheet model for continental deformation. Geophys. J. R. Astron. Soc. 70, 295–321.
England, P., Molnar, P., 1997. Active deformation of Asia: from kinematics to dynamics. Science 278, 647–650.
England, P.C., Houseman, G., 1988. The mechanics of the Tibetan Plateau. Philos. Trans. R. Soc. Lond. Ser. A 326, 301–320.
Flesch, L.M., Haines, A.J., Holt, W.E., 2001. Dynamics of the India-Eurasia collision zone. J. Geophys. Res., Solid Earth 106, 16435–16460.
Gahalaut, V.K., Gahalaut, K., 2007. Burma plate motion. J. Geophys. Res., Solid Earth 112.
Gan, W., Zhang, P., Shen, Z.K., Niu, Z., Wang, M., Wan, Y., Zhou, D., Cheng, J., 2007. Present-day crustal motion within the Tibetan Plateau inferred from GPS measurements. J. Geophys. Res., Solid Earth 112.
He, H., Oguchi, T., 2008. Late Quaternary activity of the Zemuhe and Xiaojiang faults in southwest China from geomorphological mapping. Geomorphology 96, 62–85.
Hu, X.P., Zang, A., Heidbach, O., Cui, X.F., Xie, F.R., Chen, J.W., 2017. Crustal stress pattern in China and its adjacent areas. J. Asian Earth Sci. 149, 20–28.
Kong, X., Yin, A., Harrison, T., 1997. Evaluating the role of preexisting weaknesses and topographic distributions in the Indo-Asian collision by use of a thin-shell numerical model. Geology 25, 527–530.
Leloup, P., Tapponnier, P., Lacassin, R., Searle, M., 2007. Discussion on the role of the Red River shear zone, Yunnan and Vietnam, in the continental extrusion of SE Asia Journal, Vol. 163, 2006, 1025–1036. J. Geol. Soc. 164, 1253–1260.
Leloup, P.H., Lacassin, R., Tapponnier, P., Schärer, U., Zhong, D., Liu, X., Zhang, L., Ji, S., Trinh, P.T., 1995. The Ailao Shan-Red River shear zone (Yunnan, China), Tertiary transform boundary of Indochina. Tectonophysics 251, 3–84.
León Soto, G., Sandvol, E., Ni, J.F., Flesch, L., Hearn, T.M., Tilmann, F., Chen, J., Brown, L.D., 2012. Significant and vertically coherent seismic anisotropy beneath eastern Tibet. J. Geophys. Res., Solid Earth 117.
Lev, E., Long, M.D., van der Hilst, R.D., 2006. Seismic anisotropy in Eastern Tibet from shear wave splitting reveals changes in lithospheric deformation. Earth Planet. Sci. Lett. 251, 293–304.
Li, Y.H., Liu, M., Wang, Q.L., Cui, D.X., 2018. Present-day crustal deformation and strain transfer in northeastern Tibetan Plateau. Earth Planet. Sci. Lett. 487, 179–189.
Liu, M., Yang, Y., 2003. Extensional collapse of the Tibetan plateau: results of three-dimensional finite element modeling. J. Geophys. Res., Solid Earth 108.
Liu, Q.Y., Van Der Hilst, R.D., Li, Y., Yao, H.J., Chen, J.H., Guo, B., Qi, S.H., Wang, J., Huang, H., Li, S.C., 2014. Eastward expansion of the Tibetan Plateau by crustal flow and strain partitioning across faults. Nat. Geosci. 7, 361–365.
Luo, G., Liu, M., 2010. Stress evolution and fault interactions before and after the 2008 Great Wenchuan earthquake. Tectonophysics 491, 127–140.
Ran, Y.K., 2008. Late Quaternary geomorphic deformation and displacement rates of the Anninghe fault around Zimakua. Seismol. Geol. 30, 86–98.
Replumaz, A., Tapponnier, P., 2003. Reconstruction of the deformed collision zone between India and Asia by backward motion of lithospheric blocks. J. Geophys. Res., Solid Earth 108, 2285.
Royden, L.H., Burchfiel, B.C., van der Hilst, R.D., 2008. The geological evolution of the Tibetan Plateau. Science 321, 1054–1058.
Searle, M.P., 2006. Role of the Red River Shear zone, Yunnan and Vietnam, in the continental extrusion of SE Asia. J. Geol. Soc. 163, 1025–1036.

Shen, J., Wang, Y.P., Song, F.M., 2003. Characteristics of the active Xiaojiang fault zone in Yunnan, China: a slip boundary for the southeastward escaping Sichuan–Yunnan Block of the Tibetan Plateau. J. Asian Earth Sci. 21, 1085–1096.
Shen, Z.K., Lü, J., Wang, M., Bürgmann, R., 2005. Contemporary crustal deformation around the southeast borderland of the Tibetan Plateau. J. Geophys. Res., Solid Earth 110.
Shi, X., Sieh, K., Weldon, R., Zhu, C., Han, Y., Yang, J., Robinson, S.W., 2018a. Slip rate and rare large prehistoric earthquakes of the Red River fault, southwestern China. Geochem. Geophys. Geosyst. 19, 2014–2031.
Shi, X., Wang, Y., Sieh, K., Weldon, R., Feng, L., Chan, C.H., Liu-Zeng, J., 2018b. Fault slip and GPS velocities across the Shan Plateau define a curved southwestward crustal motion around the eastern Himalayan syntaxis. J. Geophys. Res., Solid Earth 123, 2502–2518.
Shi, Y.L., Cao, J.L., 2008. Effective viscosity of China continental lithosphere. Earth Sci. Front. 15, 82–95.
Tape, C., Musé, P., Simons, M., Dong, D., Webb, F., 2009. Multiscale estimation of GPS velocity fields. Geophys. J. Int. 179, 945–971.
Tapponnier, P., Molnar, P., 1977. Active faulting and tectonics in China. J. Geophys. Res. 82, 2905–2930.
Tapponnier, P., Peltzer, G., Le Dain, A., Armijo, R., Cobbold, P., 1982. Propagating extrusion tectonics in Asia: new insights from simple experiments with plasticine. Geology 10, 611–616.
Wang, C.Y., Flesch, L.M., Silver, P.G., Chang, L.J., Chan, W.W., 2008. Evidence for mechanically coupled lithosphere in central Asia and resulting implications. Geology 36, 363–366.
Wang, E., Burchfiel, B.C., Royden, L.H., Chen, L., Chen, J., Li, W., Chen, Z., 1998. Late Cenozoic Xianshuihe-Xiaojiang, Red River, and Dali fault systems of southwestern Sichuan and central Yunnan, China. Spec. Pap., Geol. Soc. Am. 327, 1–108.
Wang, M., 2009. Analysis of GPS Data with High Precision and Study on Present-Day Crustal Deformation in China. Institute of Geology, China Earthquake Administration, pp. 1–95.
Wessel, P., Smith, W.H., Scharroo, R., Luis, J., Wobbe, F., 2013. Generic mapping tools: improved version released. Eos Trans. AGU 94, 409–410.
Xu, X.W., Wen, X.Z., Han, Z.J., Chen, G.H., Li, C.Y., Zheng, W.J., Zhnag, S.M., Ren, Z.Q., Xu, C., Tan, X.B., 2013. Lushan Ms7.0 earthquake: a blind reserve-fault event. Chin. Sci. Bull. 58, 3437–3443.
Yang, Y., Liu, M., 2010. What drives short- and long-term crustal deformation in the southwestern United States? Geophys. Res. Lett. 37.
Yang, Y., Liu, M., 2013. The Indo-Asian continental collision: a 3-D viscous model. Tectonophysics 606, 198–211.
Yin, A., 2010. Cenozoic tectonic evolution of Asia: a preliminary synthesis. Tectonophysics 488, 293–325.
Yin, A., Harrison, T.M., 2000. Geologic evolution of the Himalayan-Tibetan orogen. Annu. Rev. Earth Planet. Sci. 28, 211–280.
Yin, F., Jiang, C., Han, L., Zhang, H., Zhang, B., 2018. Seismic hazard assessment for the Red River fault: insights from Coulomb stress evolution. Chin. J. Geophys. 61, 183–198.
Zhang, P., Deng, Q., Zhang, G., Ma, J., Gan, W., Min, W., Mao, F., Wang, Q., 2003. Active tectonic blocks and strong earthquakes in the continent of China. Sci. China, Ser. D, Earth Sci. 46, 13–24.
Zhang, P.Z., Shen, Z., Wang, M., Gan, W., Bürgmann, R., Molnar, P., Wang, Q., Niu, Z., Sun, J., Wu, J., 2004. Continuous deformation of the Tibetan Plateau from global positioning system data. Geology 32, 809–812.
Zhang, P.Z., Wen, X.Z., Shen, Z.K., Chen, J.H., 2010. Oblique, high-angle, listric-reverse faulting and associated development of strain: the Wenchuan earthquake of May 12, 2008, Sichuan, China. Annu. Rev. Earth Planet. Sci. 38, 353–382.
Zhang, Q., Sandvol, E., Ni, J., Yang, Y., Chen, Y.J., 2011. Rayleigh wave tomography of the northeastern margin of the Tibetan Plateau. Earth Planet. Sci. Lett. 304, 103–112.
Zheng, G., Wang, H., Wright, T.J., Lou, Y., Zhang, R., Zhang, W., Shi, C., Huang, J., Wei, N., 2017. Crustal deformation in the India-Eurasia collision zone from 25 years of GPS measurements. J. Geophys. Res., Solid Earth 122.